Experimental and Numerical Analysis of Slurry Pot Tester by Response Surface Methodology (RSM) and Computational Fluid Dynamics (CFD)

Vineet Singh[1*], Vinod Singh Yadav[2,] Vaibhav Trivedi[3]

[1,3]Department of Mechanical Engineering, School of Engineering and Technology, IFTM University, Moradabad, Uttar Pradesh, India.

[2]National Institute Technology, Srinagar, India. Department of Mechanical Engineering, Uttarakhand, India.

*Author to whom correspondence should be addressed:
E-mail: vineet.singh@iftmuniversity.ac.in

(Received March 15, 2023; Revised April 17, 2023; accepted April 20, 2023).

Abstract: Erosion wear is a big problem in hydraulic reaction turbines and centrifugal pumps. It not only reduces the life of the turbine but also reduces the performance and power output since it removes the material from the guide vane due to that water will not reach the impeller blade at the designed blade angle. In this research paper, a slurry pot tester has been designed and manufactured in the lab to analyze the suspension of sand particles in water at a varying concentration of sand, particle size, and terminal velocity by the Response Surface Methodology (RSM) and Computational Fluid Dynamics (CFD). The RSM determines the suspension speed of sand particles based on experimental data. The CFD simulation was conducted to study the internal flow field of the sand water mixture in the slurry pot tester. For experimentation, the particle size varies from 200 μm, 325 μm, and 450 μm, sand concentration varies from 1%, 3.5%, and 6%, and terminal velocity from 0.06046 m/s, 0.08768 m/s and 0.1149 m/s. Finally, surface plots, contour plots, and factorial plots are drawn in the RSM to find the outcomes of input variables on the suspension speed. The residual plot, Analysis of Variance (ANOVA), and Pareto chart show the accuracy of the predicted results of RSM. The regression equations generated by ANOVA give good accuracy with S, R2, and R2(adj) values 0.538384, 99.99%, and 99.98%, respectively. The CFD simulation results give a good inner picture of the slurry pot tester by plotting the graph of phase distribution, path line, and velocity field.

Keywords: Slury Pot tester; Sand particle; Sand Concentration; Terminal Velocity; Optimization; Computational Fluid Dynamics (CFD).

1. Introduction

The erosion wear due to sand particles with high impact velocity is the big problem faced in the hydraulic reaction turbines and the centrifugal pump. This problem reduces the turbine's life and hampers the power produced by the turbine and the hydraulic efficiency. The guide vanes are an essential part of a hydraulic turbine because guide vanes control the flow of water at the design angle on the impeller blade so that incidence losses are low and the turbine produces the maximum power. If the material has been removed on the guide vanes due to erosion wear, the water did not reach the impeller blade at a particular design angle, increasing the incidence losses and reducing the turbine's performance. To explore the effect of erosion wear, a slully pot tester was used for experimental work. Experiment was conducted on the martensite stainless steel CA6NM at diverse orientation angles 15° to 90° at varying impact velocities[1)].

The performance of the hydraulic machines (Pump, Turbines) was drastically reduced due to these sand and slurry particles. The investigation of the slurry pump concluded that if the slurry concentration increased in the water flow, it decreased the pump's performance[2)].

erosion wear can be calculated by developing a model with low turbulence and an accurate sand or slurry particle concentration in water.

A study was conducted on a slurry pot tester to find the flow field characteristic on the model, in which a stirrer was used with the six-blade 45° pitched turbine blade[3)]. The erosion wear in the material can be reduced by creating a hard-coated surface on the guide vane surface which is in direct contact with the sand and water mixture at the inlet section of the turbine. The grey cast iron wear properties have been enhanced by the addition of magnesium, chromium, and silica over the inner surface of the turbine[4)]. The homogeneous distribution of the sand in water depends on the concentration of the sand, particle

size, turbulence inside the model, and the propeller's speed.

The Computational Fluid Dynamics (CFD) study has been conducted to investigate turbulence and sand particle distribution inside the pot tester[5]. A slurry pot tester has been designed and developed by[6] for investigating the erosion wear on the ductile material. The study was conducted on non-ferrous materials, AISI 316L, stainless steel, turbine blade steel and erodent materials chosen to be quartz, carbide, and silica. The particle impact velocity, angle, and frequency are three essential variables that govern the erosion due to slurry and sand in water on the contacting surface. A study has been conducted to find the effects of these three variables on material loss[7, 8].

The actual calculation of erosion wears is necessary to study the particle impact on the eroded surface. The Lagrangian approach has been used for investigating the outcome of velocity, impact angle, and impacting frequency on the wear rate[9]. The erosion wear in slurry pump at high impact velocity has been measured by [10]. A new, suspended particle monitoring study has been conducted. A river water sample was collected, and based on the sample, a correction factor multiplied with the results obtained by in-house experimental work [11]. The wear rate is very much affected due to material properties. The nanoparticles composites with cotton fibers reduced the wear rates significantly[12].

The speed of the propeller at which all sand particles at the bottom of the pot tester are suspended in water at minimum turbulence is known as the suspension speed. From the above literature and analysis, it is detected that the suspension speed of the particle is the most important parameter for getting the actual results of the erosion rate of the material. If the suspension speed is very high, the particle will suspend in water, but there is a high degree of turbulence created which change the particle path and impact angle of the sand particle, and an error occurs at the time of experimentation. So, suspension speed must be optimized with respect to the size of particles, concentration, and terminal. In previous research, the optimization of the suspension speed is missing. So, in my research paper, I have presented a Response Surface Methodology to optimize the slurry pot tester input settings. The predicted optimized results of RSM have been validated with the experimental and simulation results. The CFD tool is mainly used for flow visualisation and finding the sand particles' pressure field and velocity fields.

2. Experimental Set-up

To study the suspension characteristic of sand particles in water, transparent acrylic cylindrical has been used in Figure 1. A pitched turbine blade with a blade angle of 45° is mounted on the shaft, and shaft is inserted at the base of the cylinder, and power is transferred to a 1.5hp Direct Current (DC) motor. The four holes are provided on the cylinder wall at the height 80 mm,120 mm, 160 mm, and 200 mm from the bottom of the tank respectively. The diameter of the holes are 8 mm mainly used for collecting slurry samples. The four holes marked on the cylinder in which two are on the left side of the tank at 80 mm, and 160 mm from the bottom namely L1, L2 respectively, other two are R1 and R2 at its diametrically opposite on120 mm and 200mm from the bottom respectively.

The cylindrical tank (as shown in figure 1) is made transparent with acrylic material for clear visualization. The height, diameter, and thickness of the acrylic cylinder is the 300 mm, 300 mm, and 5 mm respectively.

Figure 1 Experimental Setup of slurry Pot Tester

The experimental setup of the slurry pot tester used the transparent acrylic cylinder to observe the motion of sand particles inside the cylinder at the time roation of the propeller blades. The high speed of rotation of the propeller creates the lot of turbulence inside the acrylic cylinder, which will enhance the error in the measurement of erosion wear.

The experimental work has been conducted at varying sand concentration in water and the varying the particles size. The sand concentration vary from 1 to 6% and the particle sizes vary from 200 to 450 μm.

This experimental setup is used for the measurement of wear rate in various metal specimens. The wear rate in this slurry pot tester is occur at atmospheric temperature and pressure since the temperature and pressure majorly affect the wear characteristic of the material[13].

2.1 Instrument Used

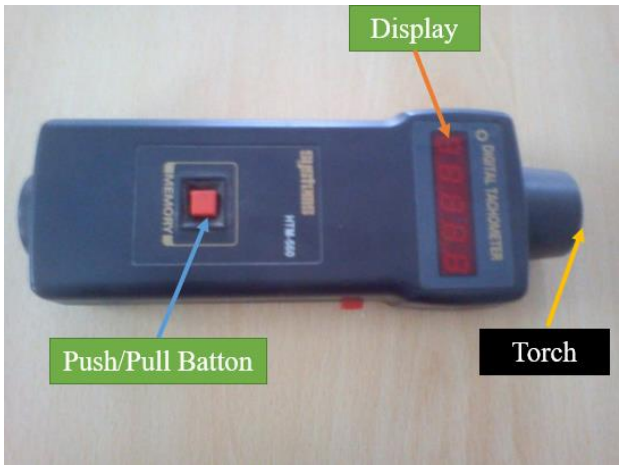

(a) Tachometer

(b) Speed regulator

(c) Electric Oven

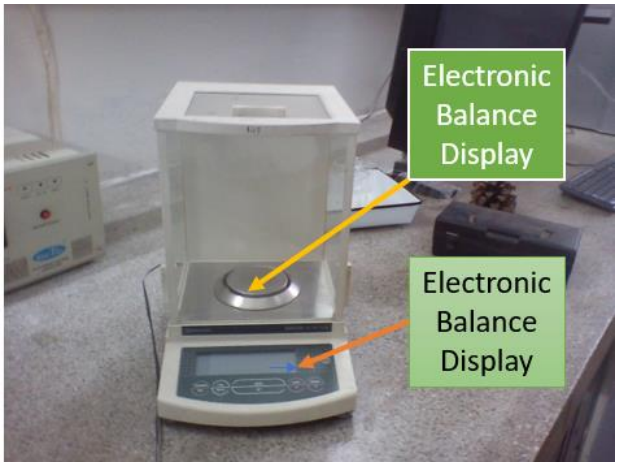

(d) Electronic balance

Figure 2: Various instruments in experimental work

Figure 2 represents the pictorial view of the instruments used in the experimental work. Figure 2 (a) shows the tachometer utilized to measure the speed of the motor without making contact with the shaft. It shows the display which shows the digital reading of the RPM of the shaft. A sticking strip is fixed on the shaft and when the laser beam falls on the strip it tracks the rotation of the strip. Figure 2 (b) shows the speed regulator which is used for varying the speed of the motor. The experiment has been started at low speed and slowly-2 speed was increased and note down the speed at which all sand particles lifted from the bottom of the tank, this speed is known as the suspension speed. Figure 2 (C) shows the electric oven, which is used to remove the moisture from the sample of sand water mixture. A knob has been provided in the electric oven which was used for changing the temperature. The beaker sample of filtered sand has been put inside the electric oven for more than half an hour and checked for any moisture left. Finally, figure 2 (d) shows the electronic balance used for measuring the weight of the sand in a sample and finding the concentration of sand at various locations in the acrylic cylinder. The electronic balance has a digital display and transparent glass housing for covering the display from atmospheric dust and dirt.

3 Method and Material

In this research, a slurry pot tester has been designed and developed for measuring the erosion wear of the different materials at a high impact velocity of around 32 m/s, but before measuring the erosion wear, it required to find the suspension speed, velocity, pressure field, and turbulence of the sand particle at the different sand concentration in water. For finding the suspension speed, the RSM tool is used to optimize the slurry pot tester and visualize the flow field. The suspension speed of the sand particles depends on the size of the particle, concentration of sand in water, and the particle's terminal velocity in water. So, in RSM, there are three input variables particle size, sand concentration, terminal velocity, and one

response variable is the suspension speed. The sand particle size, sand concentration, and particle terminal velocity varies from $200\,\mu m$, 325 µm, 450 µm, 1%, 3.5%, 6%, 0.5885 m/s, 0.6314 m/s, and 0.6641 m/s respectively.

4 Optimization Technique

The study's main purpose is to optimize the suspension speed, which depends on three input variables particle size, sand concentration, and the terminal velocity of the sand particle in water. The optimization has been completed in the Response Surface Methodology (RSM) optimization tool in MINITAB 17. The RSM is a mathematical-statistical tool which develops the relationship between the number of explanatory variables and one and more than one response variable by the regression analysis. The regression equations have been generated by the Analysis of Variance (ANOVA), a statistical approach to analyzing a complicated design depending on the several variables. The RSM used the Design of Experiments (DOE) for the matrix developed[14]. The RSM reduced the experimental time when the system depended on more than two variables. The ANOVA generates the 2nd order polymer of responses. The 2nd order model has all the ist order terms, the square of times, and the cross product of control variables represented below [15].

$$Y = A_\circ + \sum_{i=1}^{k} A_i\, x_i + \sum_{i=1}^{k} A_{ii}\, x_i^2 + \sum_{j\geq 1}^{k} A_{ij} x_i x_j + \varepsilon \quad (1)$$

Where Y represents the response and Ao is the average response, and Ai, Aii, and Aij represent the coefficient of linear, square, and cross product of the input control variables. The ε means the error or noise of response between the actual and the model data at best fit.

In this research, there are three input variables particle size, particle terminal velocity, sand concentration, and one response variable, suspension speed. In RSM Behnken Box Design (BBD) design matrix is used, which takes the value of input parameters in the form of codes. The value input variables in the form of code are represented in Table 1.

Table 1. Range of input parameters

		Code		
input parameters	**Input parameters symbols**	-1	0	1
Particle size	dp	200 µm	325 µm	450 µm
Sand concentration	C	1%	3.5%	6%
Terminal Velocity	Vt	0.06046 m/s	0.08768 m/s	0.1149 m/s

The accuracy of the results have been tested by the F Values and P values. The F values and P values are the outcomes of the prototypical analysis in ANOVA. The F values and P values represent the ANOVA coefficient in optimization. The F represents the ratio of mean sum of squares due to the treatment to the mean sum of squares due to error. The permutation test results represent by the P values. The higher F and lower P values represents the accuracy of ANOVA. Table 2 reperesents the outcomes ANOVA Table.

Table 2. Outcomes of the ANOVA model

	Suspension Speed Model	
Parameters	**F Value**	**P Value**
Model	6868.82	0.000
Linear	19724.12	0.000
square	848.66	0.000
Interaction	33.68	0.001
Lack of Fit	-	-

The maximum value of P values in Table 2 is 0.001. The low P-value represents the excellent accuracy of the optimization in RSM. It automatically deleted the values more than 0.001 by the null hypothesis because higher p Values from 0.001 has no significance. The total 15 runs is given in Table 3 as per the 3 input variables.

The response of suspension speed in terms of input variables particle size (dp), terminal velocity (Vt), and sand concentration (C) is given below in the form 2nd order polymer.

$$N_s = 113.03 + 0.0522d_p + 29.046C + 921.2V_t - 0.000052d_p^2 - 2.2558C^2 - 2799V_t^2 + 0.002093d_pC + 0.0728d_pV_t + 38.41CV_t \quad (2)$$

Where Ns is the suspension speed, dp is the particle size, C is the sand concentration (%), and Vt represents the terminal velocity of sand particles.

Table 3 Total number of run as per BBD approach of DOE

Number of Run	**Particle size(d_p)**	**Sand concentration (%)**	**Terminal Velocity (m/s)**	**Suspension speed (RPM)**
1	450	1	0.08768	206
2	325	3.5	0.08768	258.11
3	200	6	0.08768	281.5
4	325	1	0.06046	190.5
5	450	3.5	0.06046	244.31
6	325	6	0.1149	301

7	200	3.5	0.1149	267.62
8	325	1	0.1149	215
9	450	3.5	0.1149	275.8
10	200	1	0.08768	200.7
11	450	6	0.08768	290.1
12	325	6	0.06046	267.2
13	200	3.5	0.06046	237
14	325	3.5	0.08768	258
15	325	3.5	0.08768	258

The S, $R^{2,}$ and R^2 (adj) represents the accuracy of model. The S, R^2 and R^2 (adj) values for suspension speed are 0.538384,99.99%, 99.98% respectively. The response R^2 and R^2 (adj) are more than 95%, representing the good accuracy of the model. The equation (2) generated after the regression analysis.

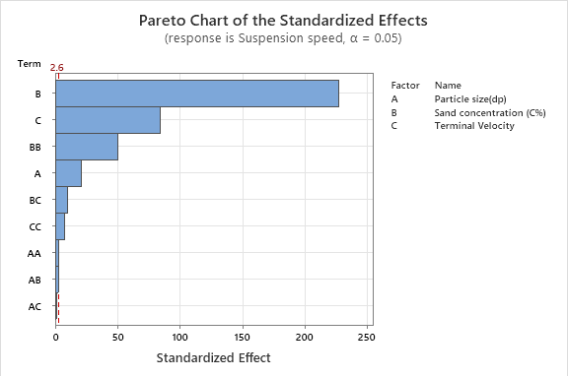

(a) Pareto Chart

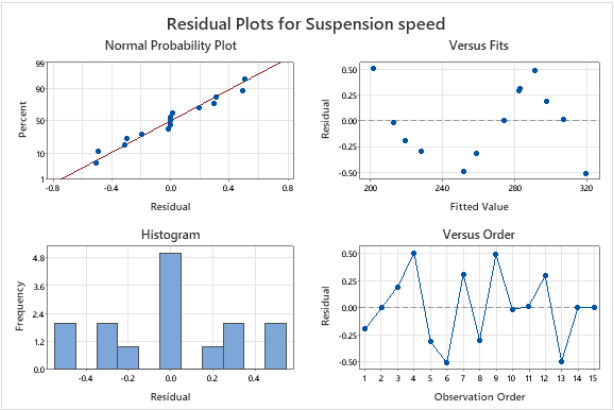

(b) Residual Plot

Figure 3: Pareto and Residual plot on suspension speed

Figures 3 (a) and (b) represents the Pareto and residual plot of the suspension speed. The Pareto chart represents the effect of control variables (particle size, sand mixture concentration, and particle terminal velocity) on the suspension speed. Figure 3(a) shows that the average standardized effect on the suspension speed is 2.6, and sand particle concentration gives the maximum standardized effect on suspension speed. The pareto chart clearly shows that the particle size standardized effect is minimum for sand particle concentration and terminal velocity[16]. Figure 3 (b) shows the residual plot as per the experimental and predicted data with observation order. The residual is obtained after subtracting the experimental and predicted results after simulation. Figure 3 (b) observed that simulation results are valid with tolerance of ± 0.5.

5. CFD Modelling

The Computational Fluid Dynamics (CFD) tool is used for determining the velocity and pressure field of sand particles in the water tank at various sand concentarion.

The conservation equations (mass and momentum) in three dimensions are basic model equations which govern the flow.

5.1 Continuity equation

In the cylindrical coordinate system, the 3D conservation of mass equation represented as follows.

$$1/r\ \partial(rur\ )/\partial r + 1/r\ \ \partial(u\theta\ )/\partial\theta + (\partial uz)/\partial z = 0 \quad (3)$$

5.2 Momentum equations

The momentum equation in three dimensions is based he newtons 2nd law. These equations are used for determing the pressure and velocity field in the 3 directions. Equations 4, 5, and 6 represent the momentum equations in X, Y, and Z directions respectively.

$$\rho\left(\frac{u\partial u}{\partial x}+\frac{v\partial u}{\partial y}+\frac{w\partial u}{\partial z}\right)=\rho g_x-\frac{\partial p}{\partial x}+\frac{\partial}{\partial x}\left(2\mu(\frac{\partial u}{\partial x}+\right.$$

$$\left.\vec{\lambda}\nabla.(\vec{V})\right)+\frac{\partial}{\partial y}(\mu\left(\frac{\partial u}{\partial y}+\frac{\partial v}{\partial x}\right)+\frac{\partial}{\partial z}(\mu(\frac{\partial u}{\partial z}+\frac{\partial w}{\partial x}) \quad (4)$$

$$\rho\left(\frac{u\partial v}{\partial x}+\frac{v\partial v}{\partial y}+\frac{w\partial v}{\partial z}\right)=\rho g_y-\frac{\partial p}{\partial y}+\frac{\partial}{\partial y}\left(2\mu(\frac{\partial v}{\partial x}+\right.$$

$$\left.\vec{\lambda}\nabla.(\vec{V})\right)+\frac{\partial}{\partial x}(\mu\left(\frac{\partial u}{\partial y}+\frac{\partial v}{\partial x}\right)+\frac{\partial}{\partial z}(\mu(\frac{\partial v}{\partial z}+\frac{\partial w}{\partial y}) \quad (5)$$

$$\rho\left(\frac{u\partial w}{\partial x}+\frac{v\partial w}{\partial y}+\frac{w\partial w}{\partial z}\right)=\rho g_z-\frac{\partial p}{\partial z}+\frac{\partial}{\partial z}\left(2\mu(\frac{\partial u}{\partial x}+\right.$$

$$\left.\vec{\lambda}\nabla.(\vec{V})\right)+\frac{\partial}{\partial y}(\mu\left(\frac{\partial v}{\partial z}+\frac{\partial w}{\partial y}\right)+\frac{\partial}{\partial x}(\mu(\frac{\partial u}{\partial z}+\frac{\partial w}{\partial x}) \quad (6)$$

The CFD simulation in post processing represents the solution of these above equation. The CFD results are based on the selection of models in simulation.

5.3 The K-ε Model

In the k-ε model, the k represents the turbulent kinetic

energy and ε represents the rate of dissipation of turbulence kinetic energy. So two equations are used for representing the total kinetic energy for the turbulent flow. One equation counted the effect of turbulent kinetic energy from total kinetic energy of the turbulent flow. The 2nd equation represents the turbulent kinetic energy due to the dissipation effect of the eddies. This model determines the turbulence intensity in the governing system which promotes the intense mixing of sand and water.

5.4 Boundary conditions

The main boundary conditions which govern the flow are as follows.

1- The no-slip boundary condition occurs on the wall.
2- The water is assumed to be turbulent inside the tank.
3- At fully turbulent flow, the flow field is assumed to be non-viscous.

The vortex motion is assumed to be absent in the tank.

6. Results and Discussion

6.1 Factorial plot of input variables

Figure 4 (a) and (b) show the variation of suspension speed versus particle size, particle concentration, and the terminal velocity of sand particles. Figure 4 (a) shows the suspension speed variation with the particle size and sand concentration[17), 18)] and terminal velocity one by one. Figure 4 (a) and Figure 4 (b) represent that if particle size, concentration, and terminal velocity increase, the suspension speed increases since the increase in particle size and sand concentration increase the drag force required for lifting the sand particle in water[19), 20)]. To increase the accuracy of measurement of erosion wear, the particle must suspend in water at low terminal velocity. So if terminal velocity increases, a higher suspension speed is required for suspending the particle in water.

6.2 Surface plot and contour plot of suspension speed with the particle size

Figure 5(a), 5(b), and 5(c) represents the surface plot of suspension speed with sand concentration and terminal velocity by holding the values of particle size from 200, 325, and 450 µm. Figure 5(d) represents the contour plot of suspension speed with the sand concentration and terminal velocity by holding the particle size value of 200 µm[21)]. Figures 5(a), 5(b), and 5(c) show that suspension speed increases with the terminal velocity and sand concentration at constant the particle size[22)]. Figure 5(d) dark green region represents the suspension speed more than 300 RPM and the dark blue region of the shows the suspension speed of lower than 200 RPM.

6.3 Surface plot and contour plot of suspension speed with the sand concentration

Figure 6(a), 6(b), and 6(C) show that the suspension speed of the slurry pot tester is enhanced if the particle size and terminal velocity are increased by holding the values of sand concentration 1%, 3.5%, and 6% respectively. Figure 6(d) represents the contour plot which represents that at 6% sand concentration, the suspension speed is 320 RPM at a large particle size and terminal speed.

6.4 Surface plot and contour plot of suspension speed with the terminal velocity

Figure 7(a), 7(b), and 7(c) shows the variation of suspension speed with the particle size and sand concentration by holding the terminal velocity. It is seen from Figures 7(a), 7(b), and 7(c) that suspension speed increased by increasing particle size and sand concentration if holding the terminal velocity from 0.08768 m/s, 0.1149 m/s, and 0.06046 m/s, respectively[23), 24)]. Figure 7(d) shows the contour plot of suspension speed with particle size and sand concentration by holding a terminal velocity value of 0.06046 m/s. Figure 7(d) shows that the upper outer periphery of the rectangle represents a suspension speed of more than 280 RPM. The bottom portion of the rectangle defined on the graph in light green color shows that the suspension speed is less than 200 RPM[25)].

6.5 CFD Results

In the slurry pot tester, the sand particles are suspended in the water uniformly at low turbulence to measure the erosion wear accurately . It is very difficult to study the turbulence characteristics experimentally, so with the CFD tools, the path line and phase of a sand particle at the different-2 height of the cylinder have to be determined. The terminal velocity of the sand particle is determined by finding the velocity field in CFD analysis. The sand water mixture in the cylinder is the axisymmetric problem this problem can be handled in 2D.

Figure 8(a), and 8(b) represent the geometry and grid generation in FLUENT- 2014. The sand water mixture in the cylinder is axis-symmetric so this problem can be solved in 2D. Grid generation is an essential part of the CFD simulation since the accuracy of the result depends on the grid's type, size, and smoothness. There are two types of grids formed in 2D problems: triangular and quadrilateral. The accuracy of a quadrilateral grid is better than triangular, so quadrilateral grids have been used for simulation, as shown in Figure 8(b). The name selection has been done in meshing part as shown in Figure 8 (b).

6.6 Distribution of sand particles and the flow field

Figure 9(a) shows the distribution of sand particles in the water at 1% sand concentration. At the time of propeller rotation in the sand-water mixture, most of the sand collected at the bottom of the cylinder near the propeller's shaft [26)], . Figure 9(a) shows only 0 to 0.0001% sand present on the bottom part of the cylinder, which is negligible and most of the sand distributed in the upper part of the cylinder, which shows the homogeneous distribution of 1% concentration sand particle in water.

Figure 9(b) shows the path lines of the silica sand particles, it can be seen from the diagram that there is a lot of turbulence near the propeller region[27),28)] but it is reduced in upper part of cylinder. Figure 9(c) shows the velocity distribution of sand particles in the cylindrical tank water. The propeller lifts the silica particles from the bottom of the tank, and after reaching the maximum height, these particles again return to the bottom of the tank at a constant terminal velocity, as seen in Figure 9(C). At the middle of the cylindrical tank, the terminal velocity is high, as shown in Figure 9(C).

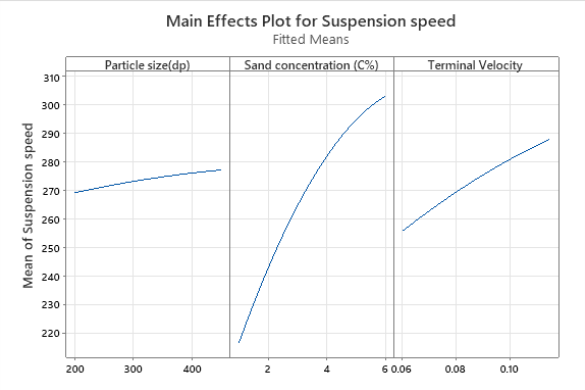

(a) Factorial plot of variation of suspension speed

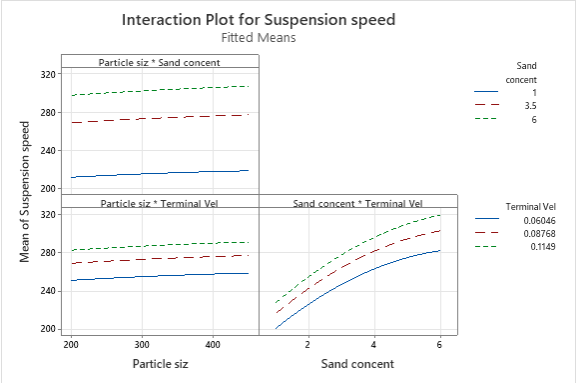

(b). Variation of suspension speed with two variables

Figure 4 suspension speed variation with input variables

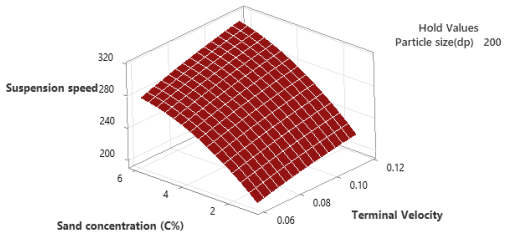

(a) Suspension speed at particle size 200 µm

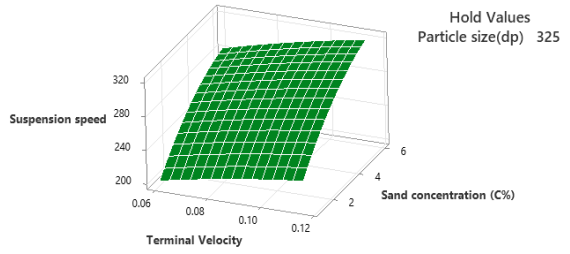

(b) Suspension speed at particle size 325 µm

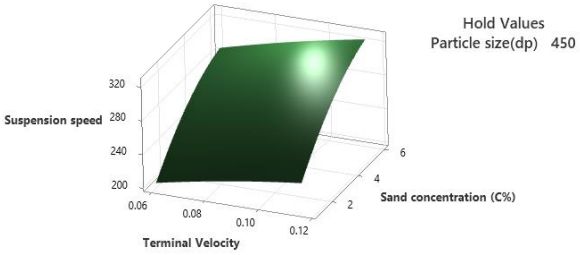

(C) Suspension speed at particle size 450 µm

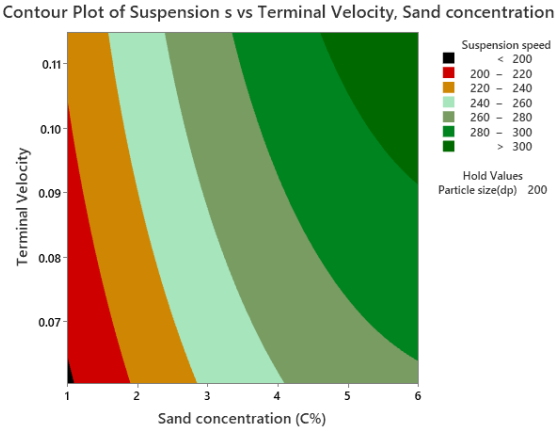

(d). Contour plot at particle size 200 µm

Figure 5 Suspension speed variation with particle size

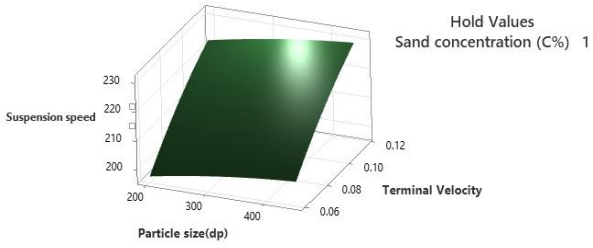

(a) Suspension speed of sand particle at sand concentration 1%

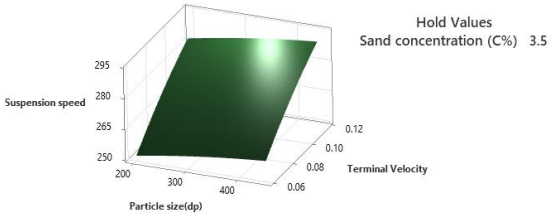

(b). Suspension speed at sand concentration of 3.5%

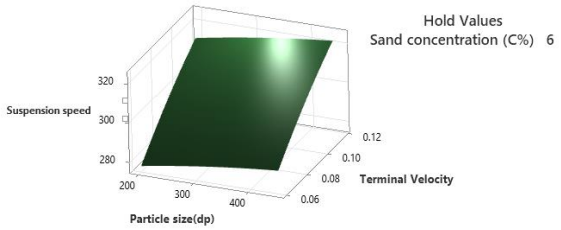

(C) Suspension speed at sand concentration 6%

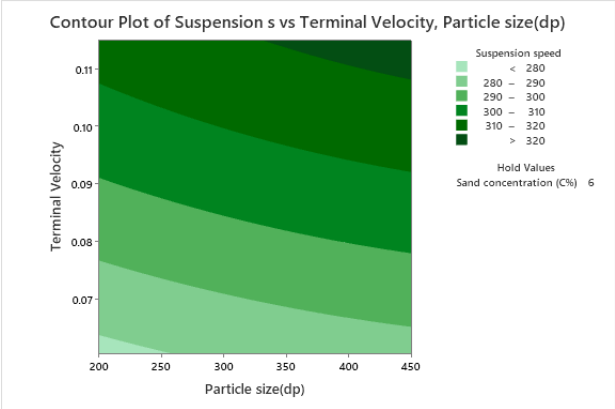

(d). Contour plot of suspension speed at 6% sand concentration

Figure 6 variation of suspension speed with terminal velocity and particle size by holding the value of sand concentration

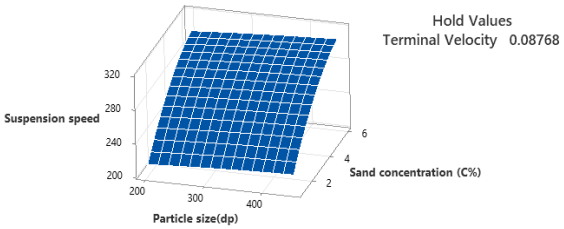

(a) Suspension speed at terminal velocity 0.08768 m/s

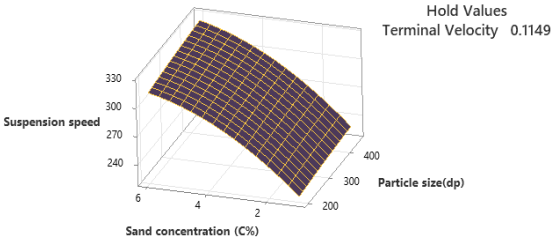

(b). Suspension speed at termial speed 0.1149 m/s

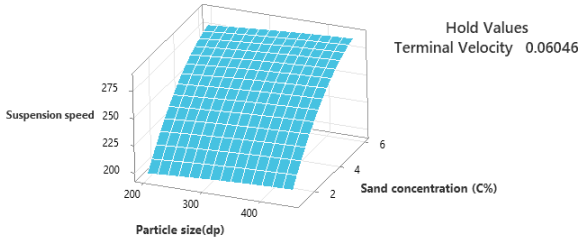

(C) Suspension speed at terminal speed 0.06046 m/s

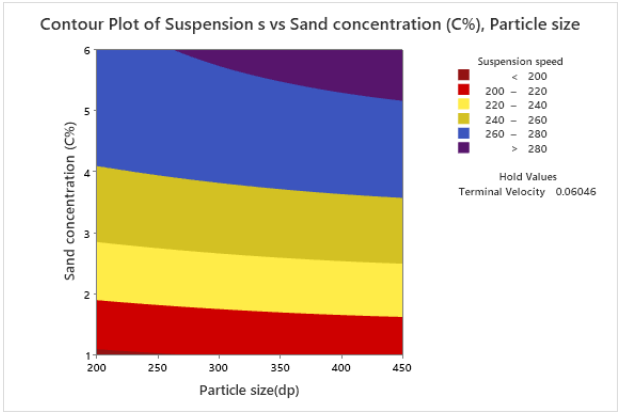

(d). Contour plot of suspension speed

Figure 7 variation of suspension speed with particle size and sand concentration by holding the value of terminal velocity

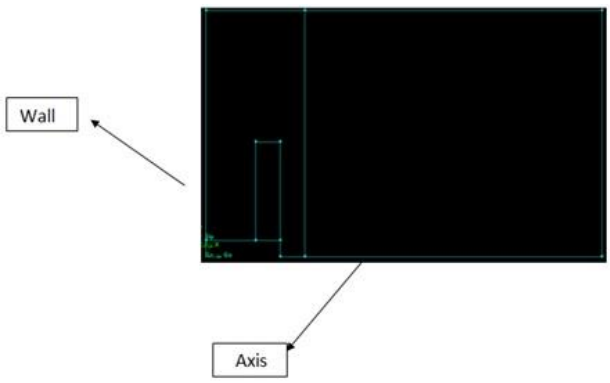

(a) The geometry of propeller and cylinder

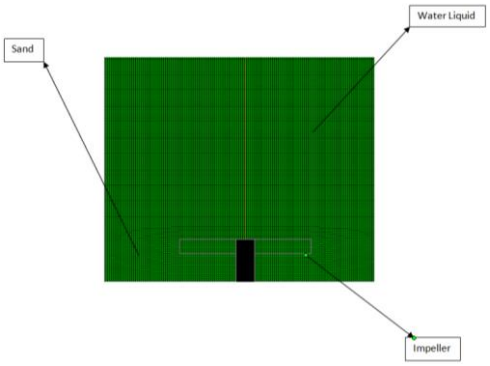

(b) Grid generation in sand water mixture

Figure 8 Geometry and grid generation in 2D Fluent

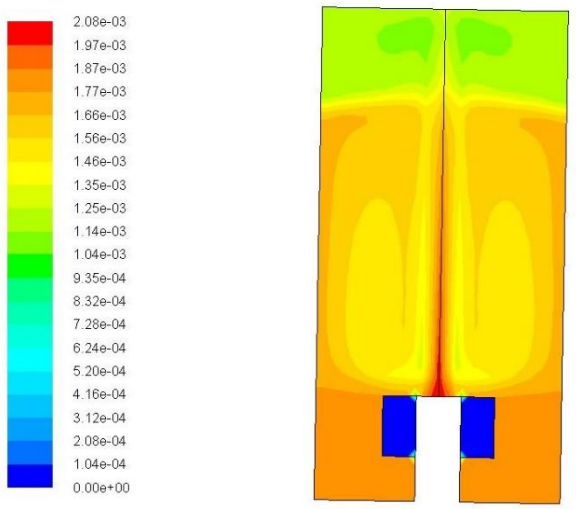

(a) Distribution of sand in water

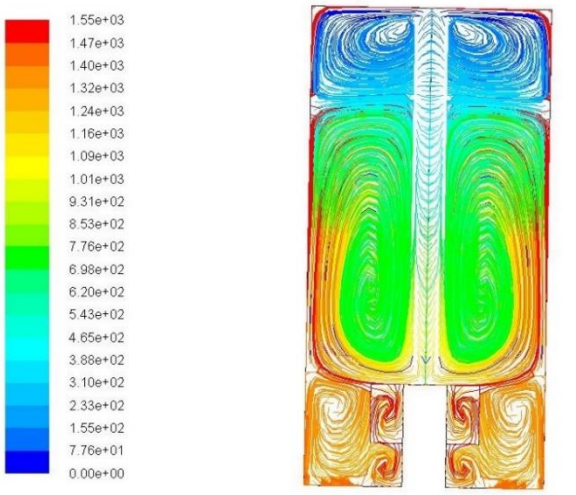

(b) Path Lines or tracking of sand particles

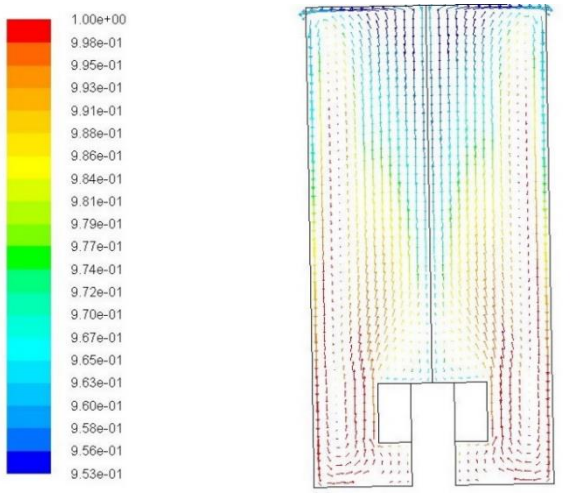

(c) Velocity field of sand particles

Figure 9 The flow field of the sand particles in water

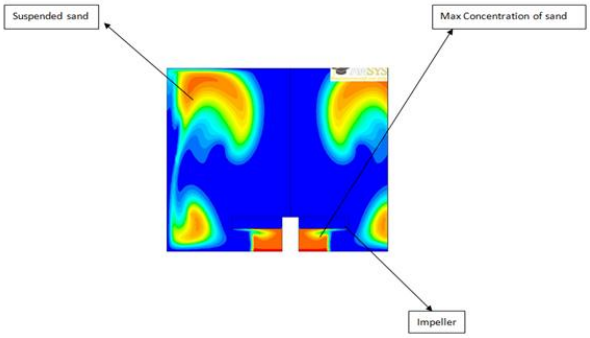

Volume fraction contour at 150 rpm 1% concentration

(a) Distribution of sand in water

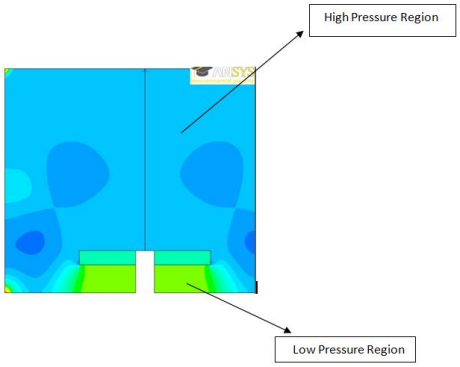

(b) Pressure field in Acrylic cylinder

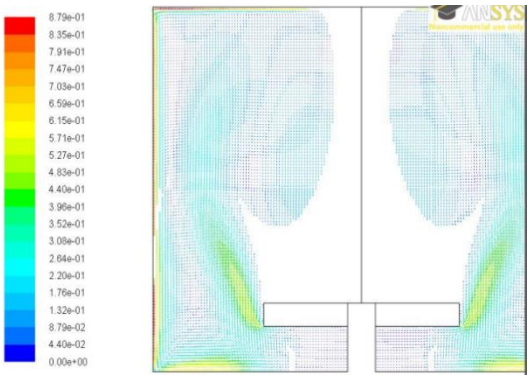

(C) Velocity field of sand particles

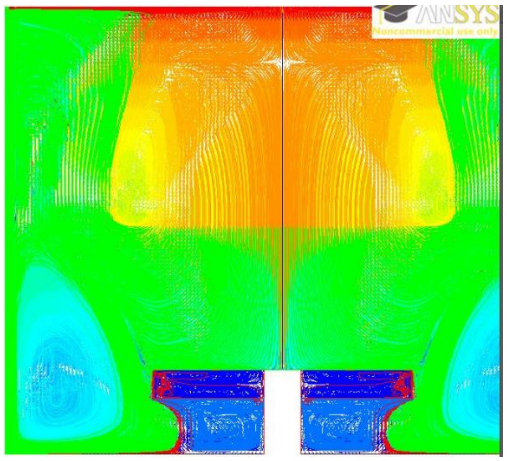

(d). Path Lines or tracking of sand particles

Figure 10: Volume contour in Acrylic cylinder

Figure 10(a), 10(b), 10(c) and represents the volume contour in the transparent cylinder. Figure 10 (a) shows the volume fraction at various locations of the cylinder. it shows from Figure 10(a) that at 150 rpm the maximum concentration of sand settles at the bottom of the cylinder, it shows nonhomogeneous mixing of sand in water. Figure 10(b) represents the pressure variation in the cylinder and it is seen that low pressure region occurs below the propeller and high pressure above the propeller. Figure 10(c) shows the velocity field which shows that at the centre line of the cylinder, no sand particle and most of the sand are moving near the periphery of the cylinder. The Figure 10(d) shows the path lines and turbulence near to propeller in the transparent cylinder.

7. Conclusion

The analysis of slurry pot tester by RSM gives the suspension speed variation with the particle size, sand concentration, and the terminal velocity. The CFD simulation results show the cylinder's inner picture by the phase distribution, path line, and velocity field. The following points are to be concluded in this resaerch.

1- The suspension speed of the sand particle in the slurry pot tester shows dependency on the particle size, sand concentration, and terminal velocity. So, the response (suspension speed) can be represented as a function of input variables (particle size, sand concentration, and terminal speed) by regression analysis represented by equation (1) [29].
2- The RSM results with the help of the Pareto chart show that the effect of terminal velocity is maximum on the suspension speed as compared to the other two parameters.
3- The particle size effect on suspension speed is not very high, but if the sand particle size increase then the suspension speed increases.
4- CFD simulation results show the pictorial view of suspension speed, if all the sand particles lift from the bottom of the sand and are suspended in water, then the propeller speed in this condition is considered to be the suspension speed as seen in Figure 9 (a). if the sand concentration in the water is high, then a higher propeller speed is required to lift all the sand from the bottom of the tank so that all particles are suspended in the water.

Nomenclature

RSM	Response Surface Methodology
DOE	Design of Experiment
CFD	Computational Fluid Dynamics
C	concentration (%)
Vt	Terminal Velocity (m/s)
dp	Particle diameter (mm)
u	Sand particle velocity in x direction (m/s)
v	Sand particle velocity in y direction (m/s)
w	Sand Particle velocity in z direction (m/s)
g_x, g_y, g_z	Gravitational acceleration in x, y and z direction (m/s^2)
ρ	Density of the fluid (Kg/m^3)
μ	Dynamic viscosity of the water (Pa.s)
P	Pressure of the fluid (Pa)

References

1) S. Sharma and B. K. Gandhi, “Erosion Wear Behavior of Martensitic Stainless Steel Under the Hydro-Abrasive Condition of Hydropower Plants,” J. Mater. Eng. Perform., vol. 29, no. 11, pp. 7544–7554, Nov. 2020, doi: 10.1007/S11665-020-05238-2.
2) B. K. Gandhi, S. N. Singh, and V. Seshadri, “Performance Characteristics of Centrifugal Slurry Pumps,” J. Fluids Eng., vol. 123, no. 2, pp. 271–280, Jun. 2001, doi: 10.1115/1.1366322.
3) B. Liu, Y. Zheng, M. Chen, X. Chen, and Z. Jin, “CFD simulation of the mixing and dispersing of floating particles in a viscous system,” Brazilian J. Chem. Eng., vol. 34, no. 4, pp. 1175–1189, Oct. 2017, doi: 10.1590/0104-6632.20170344S20160379.
4) E. E. T. ELSawy, M. R. EL-Hebeary, and I. S. E. El Mahallawi, “Effect of manganese, silicon and chromium additions on microstructure and wear characteristics of grey cast iron for sugar industries applications,” Wear, vol. 390–391, pp. 113–124, Nov. 2017, doi: 10.1016/J.WEAR.2017.07.007.
5) F. Wang, W. Wang, Y. Wang, and Z.-S. Mao, “CFD SIMULATION OF SOLID-LIQUID TWO-PHASE FLOW IN BAFFLED STIRRED VESSELS WITH RUSHTON IMPELLERS,” 2003, Accessed: Dec. 29, 2021. [Online]. Available: https://www.researchgate.net/publication/237462771.
6) G. R. Desale, B. K. Gandhi, and S. C. Jain, “Slurry erosion of ductile materials under normal impact condition,” *Wear*, vol. 264, no. 3–4, pp. 322–330, Feb. 2008, doi: 10.1016/J.WEAR.2007.03.022.
7) H. M. I. Clark, “Particle velocity and size effects in laboratory slurry erosion measurements OR… do you know what your particles are doing?,” Tribol. Int., vol. 35, no. 10, pp. 617–624, Oct. 2002, doi: 10.1016/S0301-679X(02)00052-X.
8) S. Gautam, H. P. Neopane, N. Acharya, S. Chitrakar, B. S. Thapa, and B. Zhu, “Sediment erosion in low specific speed francis turbines: A case study on effects and causes,” Wear, vol. 442–443, p. 203152, 2020, doi: 10.1016/j.wear.2019.203152.
9) K. Minemura, Y. Zhong, and T. Uchiyama, “Numerical prediction of erosion wear on pump

casing under solid-water two-phase flow conditions; Koeki nisoryuji no pump casing mamoryo no suchi yosoku," Nippon Kikai Gakkai Ronbunshu. B Hen (Transactions Japan Soc. Mech. Eng. Part B), vol. 61, 1995.

10) M. A. Rayan and M. Shawky, "Evaluation of Wear in a Centrifugal Slurry Pump:," http://dx.doi.org/10.1243/PIME_PROC_1989_203_003_02, vol. 203, no. 1, pp. 19–23, Feb. 2006, doi: 10.1243/PIME_PROC_1989_203_003_02.
11) M. Haimann, M. Liedermann, P. Lalk, and H. Habersack, "An integrated suspended sediment transport monitoring and analysis concept," Int. J. Sediment Res., vol. 29, no. 2, pp. 135–148, Jun. 2014, doi: 10.1016/S1001-6279(14)60030-5.
12) Yadav, N. K., Rajput, N. S. and Gupta, M. K. (2023) 'Investigation of the Mechanical and Wear Properties of Epoxy Resin Composite (ERCs) Made With Nano Particle TiO2 and Cotton Fiber Reinforcement', 10(01), pp. 63–77.
13) Li, Q. et al. (2022) 'Experimental investigation on the high-pressure sand suspension and adsorption capacity of guar gum fracturing fluid in low-permeability shale reservoirs: factor analysis and mechanism disclosure', Environmental Science and Pollution Research, 29(35), pp. 53050–53062. doi: 10.1007/S11356-022-19663-4/METRICS.
14) M. Hatami and D. Jing, "Optimization of wavy direct absorber solar collector (WDASC) using Al2O3-water nanofluid and RSM analysis," *Appl. Therm. Eng.*, vol. 121, pp. 1040–1050, Jul. 2017, doi: 10.1016/J.APPLTHERMALENG.2017.04.137.
15) S. J. S. Chelladurai and R. Arthanari, "Effect of stir cast process parameters on wear behaviour of copper coated short steel fibers reinforced LM13 aluminium alloy composites," Mater. Res. Express, vol. 5, no. 6, Jun. 2018, doi: 10.1088/2053-1591/AACD38.
16) K. V. Pool, C. K. H. Dharan, and I. Finnie, "Erosive wear of composite materials," Wear, vol. 107, no. 1, pp. 1–12, 1986, doi: 10.1016/0043-1648(86)90043-8.
17) J. J. Tuzson, "Laboratory slurry erosion tests and pump wear rate calculation," J. Fluids Eng. Trans. ASME, vol. 106, no. 2, pp. 135–140, 1984, doi: 10.1115/1.3243089.
18) V. Singh et al., "Experimental and Computational Investigation of Flow Fields using Accelerated Erosion Test Ring (AETR)," J. Eng. Res., Nov. 2021, doi: 10.36909/JER.ICCEMME.15599.
19) T. Itoh, A. Ikeda, T. Nagayama, and T. Mizuyama, "Hydraulic model tests for propagation of flow and sediment in floods due to breaking of a natural landslide dam during a mountainous torrent," Int. J. Sediment Res., vol. 33, no. 2, pp. 107–116, Jun. 2018, doi: 10.1016/J.IJSRC.2017.10.001.
20) M. K. Padhy and R. P. Saini, "A review on silt erosion in hydro turbines," Renew. Sustain. Energy Rev., vol. 12, no. 7, pp. 1974–1987, 2008, doi: 10.1016/j.rser.2007.01.025.
21) A. Aslam Noon and M. H. Kim, "Erosion wear on Francis turbine components due to sediment flow," Wear, vol. 378–379, pp. 126–135, 2017, doi: 10.1016/j.wear.2017.02.040.
22) S. Gohel, S. Joshi, M. Azhar, M. Horner, and G. Padron, "CFD modeling of solid suspension in a stirred tank: Effect of drag models and turbulent dispersion on cloud height," Int. J. Chem. Eng., 2012, doi: 10.1155/2012/956975.
23) S. Singh, Suraj Kumar Singh, R. Kumar, A. Shrama, and S. Kanga, "Finding Alternative to River Sand in Building Construction," Evergreen, vol. 9, no. 4, pp. 973–992, 2022, doi: 10.5109/6625713.
24) B. W. Madsen, "Measurement of erosion-corrosion synergism with a slurry wear test apparatus," Wear, vol. 123, no. 2, pp. 127–142, 1988, doi: 10.1016/0043-1648(88)90095-6.
25) Kiran S. Phad and A. Hamilton, "Experimental Investigation of Friction Coefficient and Wear of sheet metals used for Automobile Chassis," Evergreen, vol. 9, no. 4, pp. 1067–1075, 2022, doi: 10.5109/6625719.
26) Y. Xu, L. Wang, T. Chu, and D. Liang, "Suspension mechanism and application of sand-suspended slurry for coalmine fire prevention," Int. J. Min. Sci. Technol., vol. 24, no. 5, pp. 649–656, 2014, doi: 10.1016/j.ijmst.2014.03.029.
27) T. J. Hsu and P. L. F. Liu, "Toward modeling turbulent suspension of sand in the nearshore," J. Geophys. Res. Ocean., vol. 109, no. 6, pp. 1–14, 2004, doi: 10.1029/2003JC002240.
28) Pail N. Lalit, Khairnar P. Hrikesh, Hole A. J., Mate. M. D., "An Experimental Investigation of Wear Particles Emission and Noise Level from Smart Braking System," Evergreen, vol. 9, no. 3, pp. 711–720, 2022, doi: 10.5109/4843103.
29) Maurya Manish, Maurya Amrish, Kumar Sudhir, "An Overview of Recent Development and Application of Friction Stir Processing Technique," Evergreen, vol. 9, no. 3, pp. 811–829, 2022, doi: 10.5109/4843113.